Terahertz Ray Reflection Computerized Tomography

Collection Editor:
Deborah Miller

Terahertz Ray Reflection Computerized Tomography

Collection Editor:
Deborah Miller

Authors:
Deborah Miller
Warren Scott

Online:
< http://cnx.org/content/col10312/1.1/ >

C O N N E X I O N S

Rice University, Houston, Texas

Collection structure revised: December 12, 2005
PDF generated: February 4, 2011
For copyright and attribution information for the modules contained in this collection, see p. 22.

Table of Contents

Chapter 1

Introduction-Experimental Setup[1]

1.1 T-rays: appropriateness for imaging applications

Terahertz rays (T-rays) are pulses of sub- picosecond duration of electromagnetic radiation. They lie in the region on the electromagnetic spectrum between what is traditionally considered electronics and photonics. In practical implementations, picosecond bursts may be artificially generated in such a way so that they attain near linear phase and a broad fractional bandwidth in the Terahertz (THz) frequency range. Accordingly, it is possible to directly measure the temporal electric field using T- rays in a similar way that this is done for rays that lie in other regions on the electromagnetic spectrum. This allows probing depths of materials by looking at the arrival time of transmitted or reflected pulses. Note that one THz is equal to 1012 Hertz which corresponds to sub millimeter wavelengths in free space. Indeed, the wavelengths within the bandwidth of a typical T-ray are between 1 mm at 0.3 THz and 0.3 mm at 1 THz and evidently this can be translated into high temporal resolution (.3 mm in transmission and .15 in reflection), in imaging and detection applications.

[1] This content is available online at <http://cnx.org/content/m13146/1.1/>.

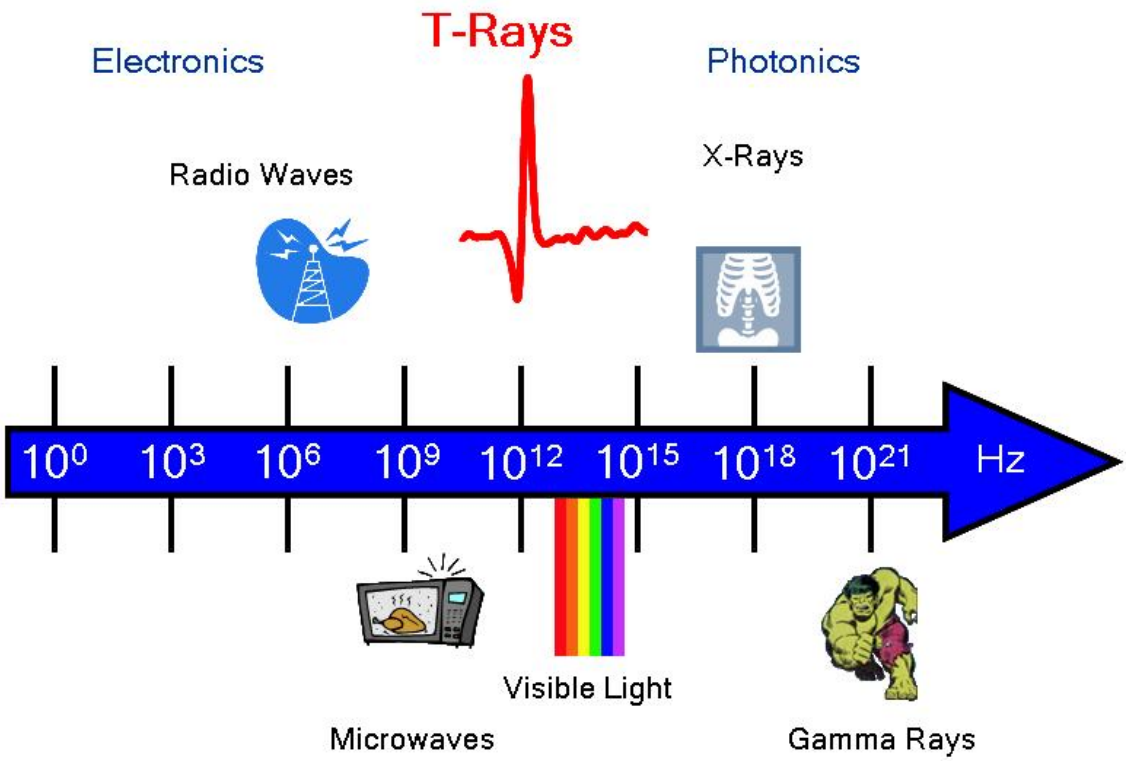

Figure 1.1

In addition, T-rays have a number of unique material responses. On the one hand, plastics, papers, and many packaging materials are virtually transparent to T-rays. In fact, plastics work with T-rays similarly to glass with visible light. As an example, all of the lenses that are used in practice to suitably focus T-rays are made out of plastic and thus they can be readily machined. On the other hand, metals, such as Aluminum, are highly reflective. Water is strongly absorbing and T-rays cannot penetrate it, rendering biomedical imaging using T-rays of limited interest. However, T-rays can be used in package inspection or for manufacturing quality control. In 1995, Hu and Nuss took the first T-ray pictures of a semiconductor (see references). This work fueled interest in using T-rays for imaging in a number of applications and in a variety of configurations. NASA is using T-rays to inspect the foam on the shuttle tanks for defects, which is believed to have caused the Columbia accident.

1.2 Experimental setup that provided the data used in this project

The present project uses experimental data obtained by a reflection computed tomography method utilizing T-rays (TRCT), proposed by J. Pearce, H. Choi, D. Mittleman, J. White, D. Zimdars (see references). In TRCT, the objective is to reconstruct the reflectivity edge map of an object's thin tomographic slice. The setup of the TRCT imaging system is shown in the next figure. A THz transceiver is used in order to generate T-ray pulses and measure the back-reflected waveforms. A lens is placed in front of the transceiver to collimate the beam and then the cylindrical lens of focal length 12 cm focuses the beam in the vertical direction, confining it to a horizontal plane. The generated T-rays illuminate a thin cross-sectional slice of the object of interest. The object is placed on a rotation stage. It is rotated in 1 degree increments for 360

degrees and a measurement is taken at each viewing angle.

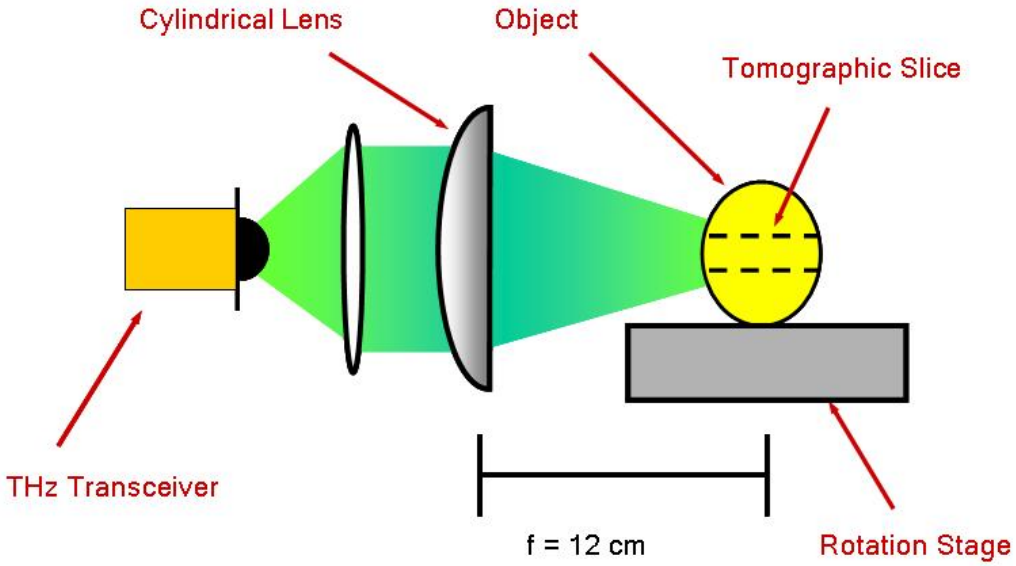

Figure 1.2

The available experimental data for the purposes of this project concern the metal square post shown in the next picture. It is a square inch in dimensions and made of aluminum. The reason for the choice of this test object is that it contains both large and small features. The dents in the metal are less than 1 mm across and it is interesting to verify the spatial resolution capabilities of the T-rays to resolve these features. Aluminum is a strong reflector so the measured reflected waveform is substantial. Since aluminum is opaque, it is not expected that the screw hole will be resolved because none of the T-rays will reach it.

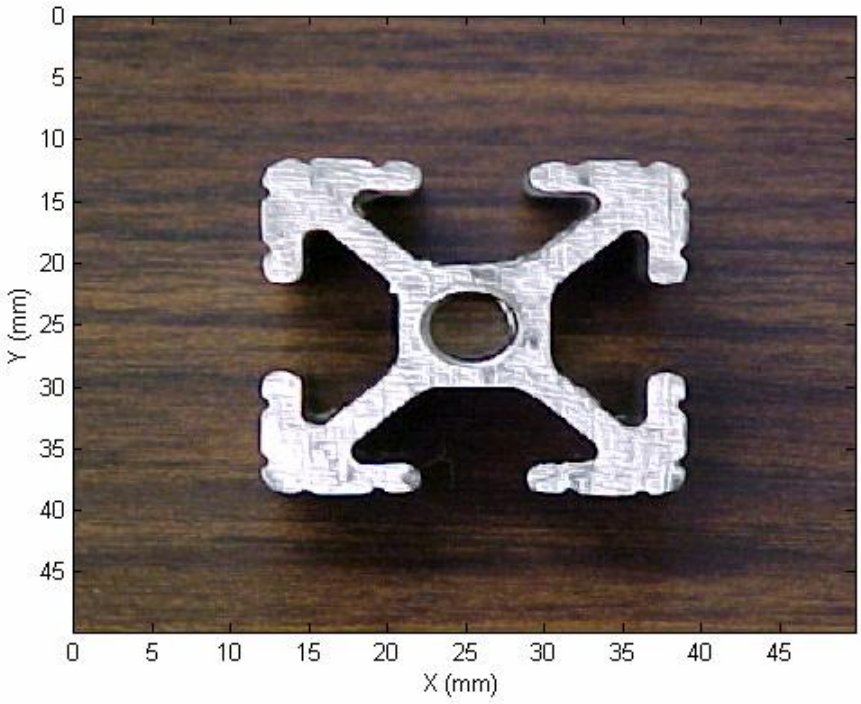

Figure 1.3

1.3 Two main steps for imaging the test object: I) Deconvolution, II) Reconstruction

The techniques and signal processing algorithms that are used are completely analogous to reflection computed tomography used with ultrasonic rays (see references). It is evident from the experimental setup that reflections from points that lie on the wavefront will sum together. This corresponds to a parallel beam projection. Each reflected waveform is the convolution of the incident T-ray pulse with the projections of the object's edge map.

The plan of attack for image retrieval consists of 2 steps. First, the projections have to be deconvolved from the measured waveforms. Second, the reflectivity map of the object is obtained from the projections. Herein, in order to deconvolve the projections from measurements, two methods were attempted: Regularized inverse filtering and Wiener filtering. Next, the image retrieval procedure is accomplished by application of the Filtered Backprojection Algorithm. FBP filters each projection with a ramp filter and then backproject the filtered projections across image plane.

Chapter 2

Description/Manipulation of Data[1]

The raw data at our disposal consisted of:

- 360 measured waveforms, one from each angle. Each waveform is a back- reflection of a transmitted THz pulse at different angles.
- The reference pulse. This is the received signal reflected off a mirror placed at the center of the turning table. We need to know the shape of the emitting pulses in order to factor out its contribution from the measured waveforms.
- The background signal. This is obtained by just receiving the noise of the environment. No pulse is emitted and no specimen is placed on the turning table.

All the above temporal signals were sampled with time step 0.016945 pico- seconds (ps) for 400 ps duration.

In the first plot of figure 1 an example waveform (measured at 70 degrees) is plotted against the reference pulse and the background signal. Clearly, both the waveform and the pulse follow the trend of the background signal. This suggests that the background signal should be first subtracted from the reference pulse and all waveforms, before any other signal processing takes place. The second plot of the same figure shows the reference and the example waveform after subtracting the environmental interference. It should be noted that the background signal is mainly a result of random mechanical vibration of the transceiver and experiment setup, plus the environmental noise that always exists.

An important observation on the second plot is that the reference pulse attains its maximum value just before 200 ps. This shows that it takes nearly 200 ps for the THz pulse to travel from the transceiver to the middle of the table and back. Moreover, the example waveform reaches the first local maximum at around 120 ps, which identifies the closest edge of the specimen.

The initial part of the example waveform consists of only high frequency and very low magnitude noise. This is the case for all the measured waveforms, although the length of the initial noisy part differs. The noise exhibited in the initial parts is representative of the noise present throughout all the waveform observations. Thus, it may serve as data to estimate the variance of the noise. The estimated variance for all the waveforms assuming Gaussian white noise ranges from 10-6∼10-7. This verifies that the level of noise is very low as can be seen in the example waveform and in the reference pulse.

[1] This content is available online at <http://cnx.org/content/m13145/1.1/>.

Reference and example waveforms

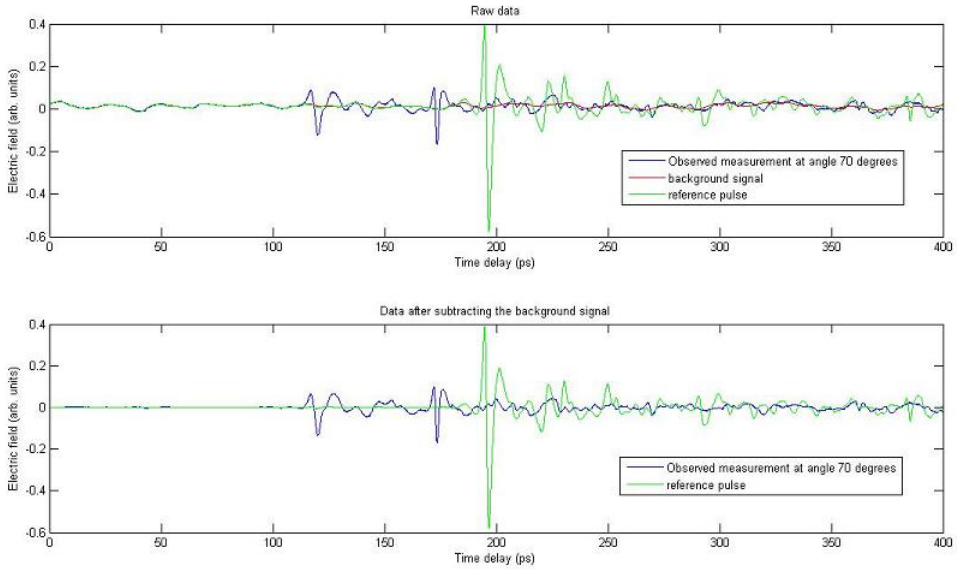

Figure 2.1

Chapter 3

Deconvolution with Inverse and Weiner Filters[1]

3.1 Problem Statement

The first task is to deconvolve the reference pulse from all the measured waveforms to obtain the actual projections of our specimen. In general the deconvolution[2] problem can be modeled as in the following figure.

Block diagram of our system

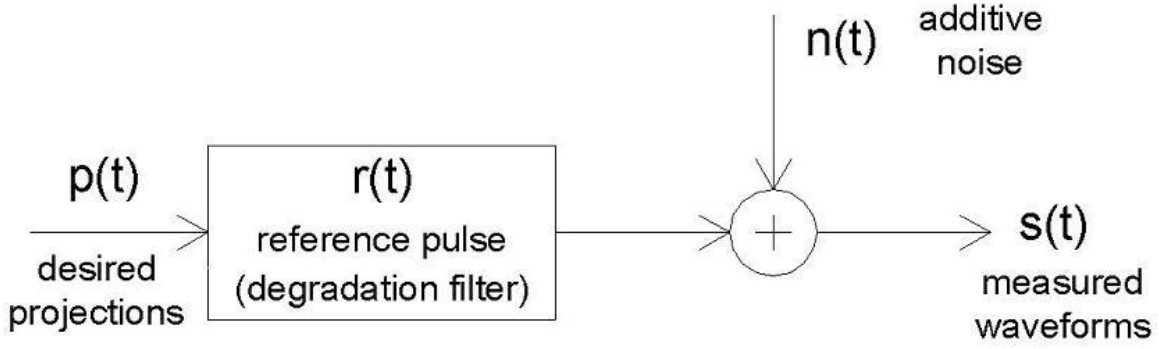

Figure 3.1

In the above figure, p(t) is the projection of the object slice that is to be used in the object reconstruction. The reference pulse is denoted by r(t) and interpreted as a low- pass degradation filter that convolves with the projections. The result of this convolution plus an additive noise n(t) is the measured waveforms s(t). In this case, both r(t) and s(t) are known and the goal is to obtain p(t) by deconvolving r(t) from s(t) and

[1] This content is available online at <http://cnx.org/content/m13144/1.2/>.
[2] "Deconvolution Basics" <http://cnx.org/content/m12472/latest/>

denoising. Mathematically the above block diagram can be written as:

$$S(\theta,t)=\int r(t-2u/c)\,p_{\theta}(u)du$$

Figure 3.2

3.2 Inverse Filter

Most of deconvolution schemes are implemented in the frequency domain. This makes sense since convolution in the time domain is mapped as multiplication in the frequency domain. Inverse filtering[3] is the simplest and most naïve method for deconvolution. No denoising takes place in this case.

Equation 1 can be written in the frequency domain as:

$$S(\omega)=R(\omega)P(\omega)$$

Figure 3.3

where S(ω), R(ω) and P(ω) are the Fourier transforms of s(t), r(t) and p(t) respectively.

$$P(\omega)=\frac{S(\omega)}{R(\omega)}$$

Figure 3.4

The main drawback of the method is that R(ω) is usually a low-pass filter and therefore $1/\mathrm{R}(\omega)$ is a high-pass filter which attains large values as the frequency increases. Thus, equation (3) becomes numerically unstable for small R(ω) values and greatly amplifies the high- frequency noise contribution. This makes inverse filtering very sensitive to even the small amounts of high frequency noise which exists in the measured waveforms.

One method of decreasing the noise sensitivity inherent when inverse filtering is to bound the frequency response $1/\mathrm{R}(\omega)$ to some threshold γ as follows:

[3] "Inverse Filters" <http://cnx.org/content/m12182/latest/>

$$G(\omega)=\begin{cases}\dfrac{1}{R(\omega)}, & \text{if } \dfrac{1}{|R(\omega)|}<\gamma \\ \gamma\dfrac{|R(\omega)|}{R(\omega)}, & \text{otherwise}\end{cases}$$

Figure 3.5

The code that implements inverse filtering is inverseFilter.m[4]

3.3 Wiener Filter

One of the most widely used restoration techniques is the Wiener filter[5]. Contrary to the inverse filtering this method also attempts to diminish noise while restoring the original signal. It executes an optimal balance between inverse filtering and noise smoothing in the mean square error sense. Assuming white Gaussian noise, the Wiener filter expressed in the Fourier domain is written as:

$$W=\frac{R(\omega)^{*}S_{pp}(\omega)}{|R(\omega)|^{2}S_{pp}(\omega)+\sigma n^{2}}$$

Figure 3.6

where Spp(ω) is the power spectrum of the input projection and σ2 is the variance of the Gaussian noise. The derivation of this formula is based on a stochastic framework and is beyond the scope of this project.

In this case the projections are unknown and an estimate of Spp is needed. This is provided by noting that Sss(ω)= Spp(ω)•|R(ω)|2, solving for Spp(ω) and substituting into equations (5) to get:

$$W=\frac{S_{ss}(\omega)}{S_{ss}(\omega)+\sigma n^{2}}\cdot\frac{1}{R}$$

Figure 3.7

[4]http://cnx.org/content/m13144/latest/inverseFilter.m
[5]"The Wiener Filter" <http://cnx.org/content/m12522/latest/>

Interestingly, the last equation can be interpreted as two different filters in cascade in the frequency domain. The first is denoising, while the second is exactly the inverse filter considered in the previous section.

The code that implements Wiener filtering is wienerFilter.m [6] .

Driver for filters[7]

[6] http://cnx.org/content/m13144/latest/wienerFilter.m
[7] http://cnx.org/content/m13144/latest/Deconvo_script.m

Chapter 4

Results of Deconvolution[1]

For the purposes of this project, much experimentation was performed in order to define the value for the threshold γ that gives the best results for both inverse and Wiener filtering methods. In addition, much effort was put forth to obtain a meaningful estimate for the variance of the noise under the Gaussian white noise assumption. To this point, one criterion for the effectiveness of each method is subjective observation of the deconvolved waveforms as opposed to the measured ones. The first plot in the following figure is the previously used example measured waveform. The next two plots show the deconvolved waveform (estimate of projection at angle 70), using the inverse and Wiener filter algorithms with appropriate parameters.

Original, inverse filtered, and weiner filtered signals

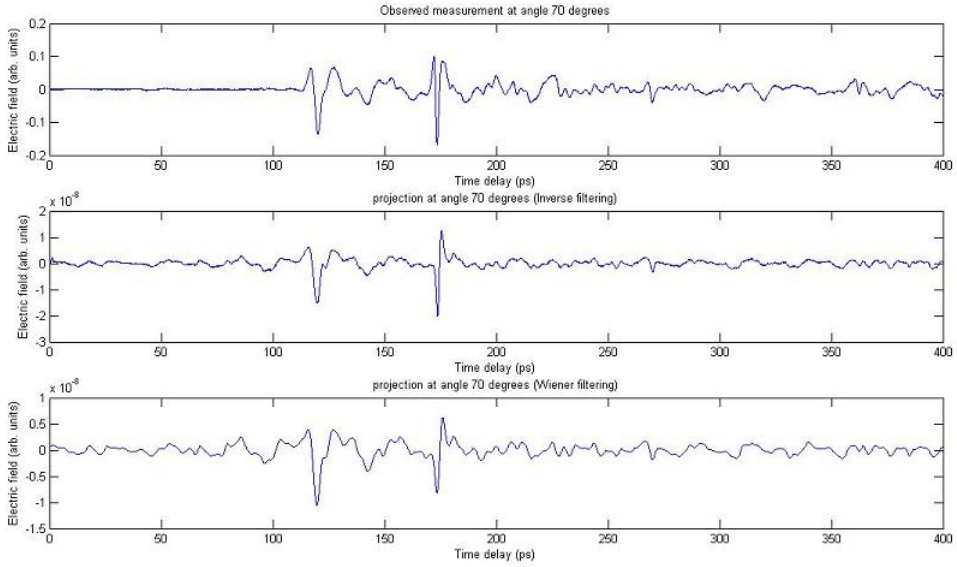

Figure 4.1

Certain conclusions can be drawn from the above plots. At first, it is evident that the patterns of the

[1]This content is available online at <http://cnx.org/content/m13148/1.1/>.

reference THz pulse signal are attenuated from the waveform after the deconvolution process in both cases. This makes the main two pulses of the measured waveform signal (occurring at about 120 and 175 ps), more distinct from the rest of the signal's features. Intuitively, this will result in a sharper image after reconstruction. Secondly, in the case of the Wiener filtered signal the absence of high frequency noise is obvious. However, since this method balances between inverse filter and noise reduction, the inverse filtering part is weaker. Overall, just inverse filtering the waveforms turns out to give better results and by appropriately choosing the γ constant the noise level is kept at negligible level. Note that after deconvolution the absolute magnitude of the signal is greatly reduced, but this is not an issue for the purpose of reconstruction since relative reflectivity values are used.

A second global criterion is a two dimensional plot of the measured and the deconvolved waveforms as a function of delay and angles. These sorts of plots are often called sinograms because of the sinusoidal behavior of the features. Each sinogram has 360 columns so that each column is a temporal plot of the estimated projections.

Sinograms of original, inverse filtered, and weiner filtered signals

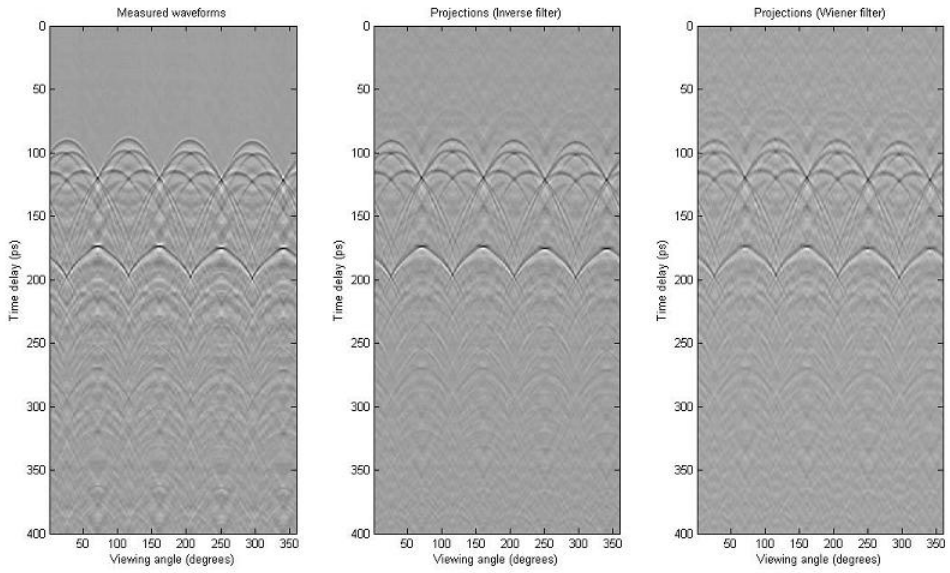

Figure 4.2

Both deconvolved sinograms exhibit sharper main sinusoid patterns, while the ripples behind them are less evident than those observed in the measured waveform sinogram.

Chapter 5

Reconstruction[1]

5.1 Theory of Filtered Backprojection Algorithm (FBP)

The FBP algorithm allows us to take the projections, P(t), developed in the previous sections and reconstruct the original image, f(x,y).

A key idea is the Fourier Slice Theorem. It says that the Fourier Transform of a projection at an angle theta is equivalent to the values of the 2-dimensional Fourier Transform of the image evaluated along a radial line of the same angle. Knowing this fact, we are able to obtain the Fourier Transform of the image, F(u,v), from projections taken at multiple angles.

We start with 2-dimensional Inverse Fourier Transform:

$$f(x,y) = \int_{-\infty}^{\infty}\int_{-\infty}^{\infty} F(u,v)e^{j2\pi(ux+vy)}dudv$$

Figure 5.1

Since we have projections for given angles, a change to polar coordinates is useful.

$$f(x,y) = \frac{1}{4\pi^2}\int_{-\infty}^{2\pi}\int_{-\infty}^{\infty} F(\omega,\theta)e^{j2\pi\omega(x\cos\theta+y\sin\theta)}\omega d\omega d\theta$$

Figure 5.2

Using symmetry, this simplifies to:

[1] This content is available online at <http://cnx.org/content/m13147/1.1/>.

$$f(x,y) = \int_0^{\pi} \int_{-\infty}^{\infty} F(\omega,\theta)|\omega| e^{j2\pi\omega t} d\omega d\theta$$

Figure 5.3

Using the Fourier Slice Theorem, we substitute in the Fourier Transform of the projection, S(ω).

$$f(x,y) = \int_0^{\pi} \int_{-\infty}^{\infty} S_{\theta}(\omega)|\omega| e^{j2\pi\omega t} d\omega d\theta$$

Figure 5.4

With this formula, we are now able to reconstruct the original image. We now see that that the FPB algorithm has certain benefits. We can begin reconstructing the image after the first projection has been calculated, since the image is built up by summing over all the angles. This could increase speed and practicality for real time applications.

Chapter 6

Backprojection Implementation[1]

Our implementation uses three pieces of Matlab code: shrinkPR, filtersinc, and backproject.

6.1 ShrinkPR

The original projection data was greatly over-sampled, taking over 20,000 samples in 400 picoseconds for each of the 360 angles. In order to reduce computation time, we uniformly reduced the number of samples and the number of angles. Our shrinkPR code takes the original PR matrix, a matrix whose columns are the projections, and outputs a smaller PR matrix with fewer samples and angles. It also creates a column vector, theta, which contains the angles of the corresponding projections.

6.2 Filtersinc

This code takes in the PR matrix and outputs the filtered PR matrix.

$$Q_\theta(t) = \int_{-\infty}^{\infty} S_\theta(\omega) |\omega| e^{j2\pi\omega t} d\omega$$

Figure 6.1

It creates the ramp filter $|\omega|$ and multiplies it with the FFT of each projection. It then takes the IFFT of each filtered projection.

6.3 Backproject

Backproject implements the discrete approximation of :

[1] This content is available online at <http://cnx.org/content/m13142/1.1/>.

$$f(x,y)=\int_0^{\pi} Q_\theta(x\cos\theta+y\cos\theta)d\theta \approx \frac{\pi}{k}\sum_{i=1}^{k} Q_{\theta i}(x\cos\theta_i+y\cos\theta_i)$$

Figure 6.2

This code backprojects each of the filtered projections over the image plane and sums them together to produce the final reconstructed image. In order to implement the continuous function given discrete data points, the "round" function was used, effectively interpolating the data.

6.4 Representative Results

The following are reconstructed images:

1500 samples per projection and 360 angles:

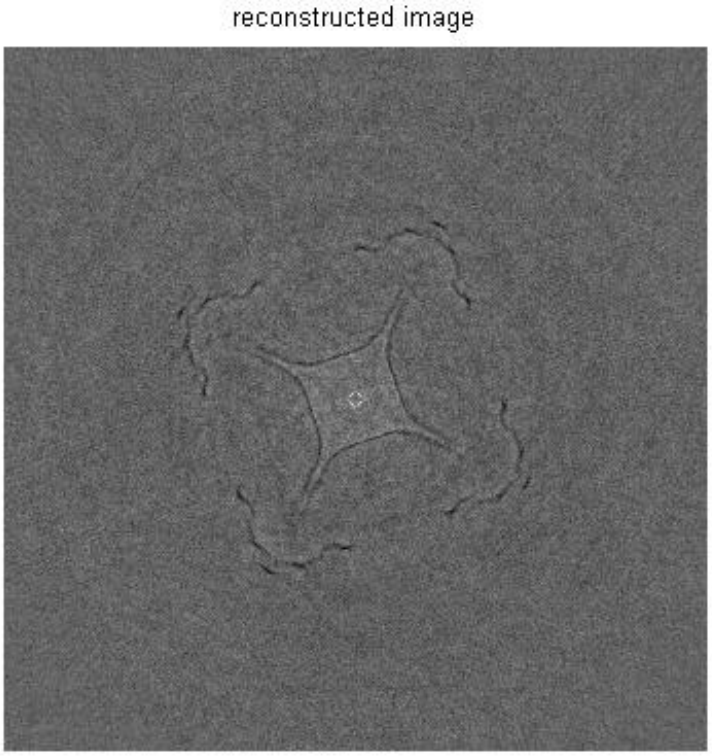

Figure 6.3

From this image you can easily see the original object.

1100 samples per projection and 360 angles:

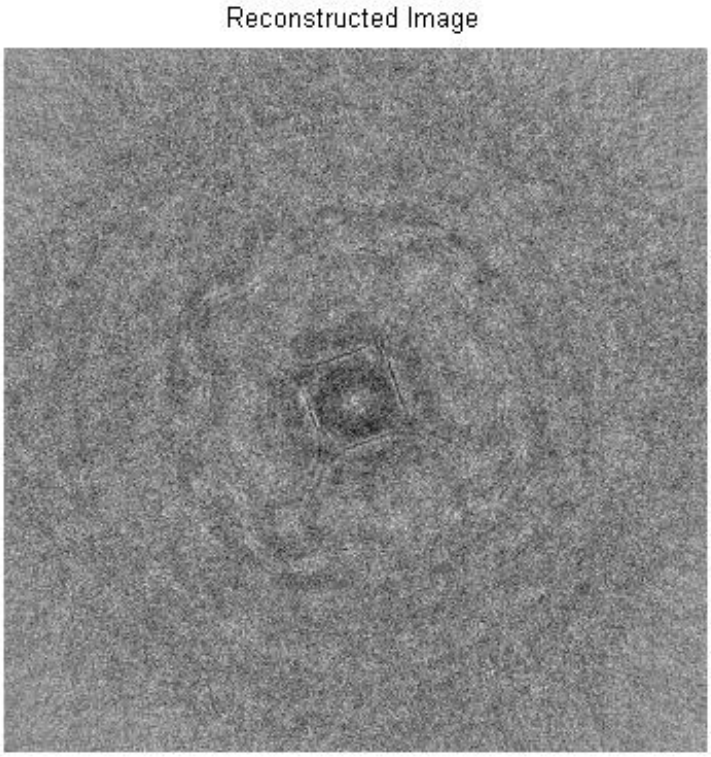

Figure 6.4

This image is not as clear since fewer samples were used.
1500 samples and angles 1-180.

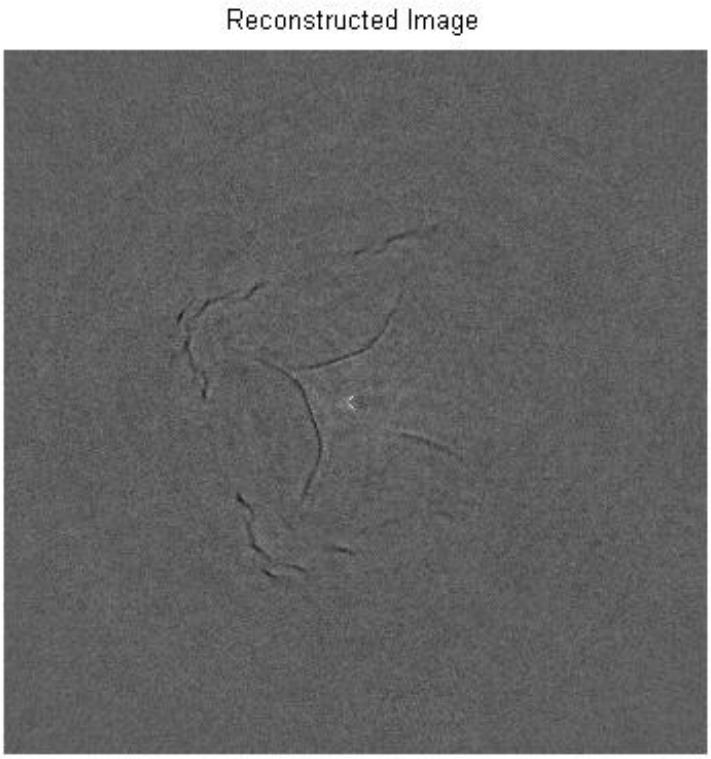

Figure 6.5

From this image you can see the left half of the object since we used the first half of the projections.

Chapter 7

Conclusions and References[1]

7.1 Conclusions

Using the terahertz reflected waveforms, we were able to measure the projections and reconstruct the original image. This process was completed in two steps. In the first, inverse and Wiener filtering were used to deconvolve the data from the reference pulse to obtain the actual projections of the test object. In the second, the Filtered Backprojection Algorithm featuring the Fourier Slice Theorem was used to filter the projections using a ramp filter and backproject the result over the image plane, thus reconstructing the image of the object.

As far as the deconvolution part of the project concerns, the regularized inverse filter gives better results than Wiener filtering, as already pointed out. Care should be exercised when picking the regularized parameter γ, so as not to increase the noise level of the resulting signal. Usually, this is a case-dependent procedure that takes numerical experimentation. It should be noted that the original data at hand were of very good quality with low noise level. Thus the results of Wiener filtering were worse than those obtained by inverse filtering.

For the reconstruction part, it was found that the number of projection angles used was vital to the clarity of the final image. We were able to greatly downsample the data and still maintain image quality to a certain point. Due to the size of the data, the algorithms ran for minutes.

7.2 Future Work

Much potential for future improvement and implementation is possible using this method of computerized tomography. Advanced deconvolution methods featuring wavelets for efficient noise reduction can be used for isolating the projections out of the measured waveforms. Furthermore, it seems reasonable to cut-off the first part of each measured waveform since it only contains noise and no useful information for the image reconstruction. This can be accomplished by appropriately windowing the raw measurements before any other manipulations takes place. Due to the linear nature of the process, different algorithm code could have been written to start reconstructing the image immediately after the first projection had been calculated. This and other efficiency tools could be implemented to greatly increase the speed of the overall reconstruction, making the process applicable for real-time use.

7.3 References

J. Pearce, H. Choi, D. M. Mittleman, J. White, and D. Zimdars, Opt. Lett. 30, 1653 (2005).

A. C. Kak and M. Slaney, Principles of Computerized Tomographic Imaging (IEEE Press, 1988).

[1] This content is available online at <http://cnx.org/content/m13143/1.1/>.

J. S. Lim, Two- Dimensional Signal and Image Processing (Prentice- Hall Inc., 1990).
D. M. Mittleman, S. Hunsche, L. Bovin, and M. C. Nuss, Opt. Lett. 22, 904 (1997).
B. B. Hu and M. C. Nuss, Opt. Lett., 20, 1716 (1995).

Chapter 8

Team Incredible[1]

Agathoklis Giaralis[2] is a Civil and Environmenal Engineering PhD candidate.

Paul Campbell [3] is an electrical engineering, economics and pre-med junior at Martel College.

Warren Scott [4] is an electrical engineering and economics junior at Martel College. He is the son of the famous statistics professor Dr. Scott.

Debbie Miller [5] is a CAAM senior from Will Rice College.

[1] This content is available online at <http://cnx.org/content/m13149/1.1/>.
[2] http://www.ruf.rice.edu/~agavader
[3] http://www.owlnet.rice.edu/~pcsoup
[4] http://www.owlnet.rice.edu/~wscott
[5] http://www.owlnet.rice.edu/~dmiller7

Attributions

Collection: *Terahertz Ray Reflection Computerized Tomography*
Edited by: Deborah Miller
URL: http://cnx.org/content/col10312/1.1/
License: http://creativecommons.org/licenses/by/2.0/

Module: "Introduction-Experimental Setup"
By: Deborah Miller, Warren Scott
URL: http://cnx.org/content/m13146/1.1/
Pages: 1-4
Copyright: Deborah Miller, Warren Scott
License: http://creativecommons.org/licenses/by/2.0/

Module: "Description/Manipulation of Data"
By: Deborah Miller, Warren Scott
URL: http://cnx.org/content/m13145/1.1/
Pages: 5-6
Copyright: Warren Scott
License: http://creativecommons.org/licenses/by/2.0/

Module: "Deconvolution with Inverse and Weiner Filters"
By: Deborah Miller, Warren Scott
URL: http://cnx.org/content/m13144/1.2/
Pages: 7-10
Copyright: Deborah Miller, Warren Scott
License: http://creativecommons.org/licenses/by/2.0/

Module: "Results of Deconvolution"
By: Deborah Miller, Warren Scott
URL: http://cnx.org/content/m13148/1.1/
Pages: 11-12
Copyright: Deborah Miller, Warren Scott
License: http://creativecommons.org/licenses/by/2.0/

Module: "Reconstruction"
By: Deborah Miller, Warren Scott
URL: http://cnx.org/content/m13147/1.1/
Pages: 13-14
Copyright: Deborah Miller, Warren Scott
License: http://creativecommons.org/licenses/by/2.0/

Module: "Backprojection Implementation"
By: Deborah Miller, Warren Scott
URL: http://cnx.org/content/m13142/1.1/
Pages: 15-18
Copyright: Deborah Miller, Warren Scott
License: http://creativecommons.org/licenses/by/2.0/

Module: "Conclusions and References"
By: Deborah Miller, Warren Scott
URL: http://cnx.org/content/m13143/1.1/
Pages: 19-20

Module: "Team Incredible"
By: Deborah Miller, Warren Scott
URL: http://cnx.org/content/m13149/1.1/
Page: 21

About Connexions

Since 1999, Connexions has been pioneering a global system where anyone can create course materials and make them fully accessible and easily reusable free of charge. We are a Web-based authoring, teaching and learning environment open to anyone interested in education, including students, teachers, professors and lifelong learners. We connect ideas and facilitate educational communities.

Connexions's modular, interactive courses are in use worldwide by universities, community colleges, K-12 schools, distance learners, and lifelong learners. Connexions materials are in many languages, including English, Spanish, Chinese, Japanese, Italian, Vietnamese, French, Portuguese, and Thai. Connexions is part of an exciting new information distribution system that allows for **Print on Demand Books**. Connexions has partnered with innovative on-demand publisher QOOP to accelerate the delivery of printed course materials and textbooks into classrooms worldwide at lower prices than traditional academic publishers.